Engineering 2D→2D parallel interpenetration using long alkoxy-chain substituents

Srboljub Vujovic, Edwin C. Constable, Catherine E. Housecroft,* Collin D. Morris, Markus Neuburger and Alessandro Prescimone

Department of Chemistry, University of Basel, Spitalstrasse 51, 4056-Basel, Switzerland

Fax: +41 61 267 1018; E-mail: catherine.housecroft@unibas.ch

Abstract

The structural consequences of reducing the length of the alkoxy substituents on going from the ditopic ligand 1,4-bis(*n*-octoxy)-2,5-bis(4,2':6',4''-terpyridin-4'-yl)benzene (**1**) to 1,4-bis(methoxy)-2,5-bis(4,2':6',4''-terpyridin-4'-yl)benzene (**2**) on reactions of the ligands with zinc(II) halides are described. Reaction of **1** with $ZnBr_2$ under conditions of room temperature crystallization gives $[\{Zn_2Br_4(\mathbf{1})\}]_n$ in which **1** acts as a planar 4-connecting node. 2D→2D parallel interpenetrated (4,4)-nets assemble; extended octoxy chains are aligned through the sheets. Replacing the octoxy tails by methoxy groups results in loss of the interpenetrated network. The coordination polymers $[\{Zn_2Br_4(\mathbf{2})\}\cdot 2C_6H_4Cl_2]_n$ and $[\{Zn_2I_4(\mathbf{2})\}\cdot 2.3C_6H_4Cl_2]_n$ consist of 2-dimensional (4,4)-nets in which the methoxy substituents are directed above and below the sheet; corrugated sheets pack with the 4,2':6',4''-tpy domains of adjacent sheets engaging in face-to-face π-interactions.

Keywords: 4,2':6',4''-terpyridine; coordination network; interpenetration; alkoxy substituents; zinc halides

1. Introduction

The recent growth in the coordination chemistry of 4,2':6',4"-terpyridine (4,2':6',4"-tpy) ligands has encompassed molecular tectons with and without coordinatively non-innocent domains in the 4'-position (Scheme 1) [1–19]. 4'-Substituents which can facilitate the assembly of 3-dimensional architectures are easily introduced during the synthesis of 4,2':6',4"-tpy using Kröhnke [20] or one-pot [21] strategies. Simpler 4,2':6',4"-tpy tectons typically bind metal ions only through the outer pyridine rings of the tpy domain (Scheme 1, left) to produce, most commonly, 1-dimensional chains. An alternative strategy for increasing the dimensionality of the coordination architecture is to design multitopic 4,2':6',4"-tpy ligands. However, despite the successful use of polytopic 2,2':6',2"-tpy ligands for the construction of multinuclear assemblies [22–27] or for enhancing electronic communication between metal centres [28,29], little attention has been paid to the coordination potential of multitopic 4,2':6',4"-tpys [30–33].

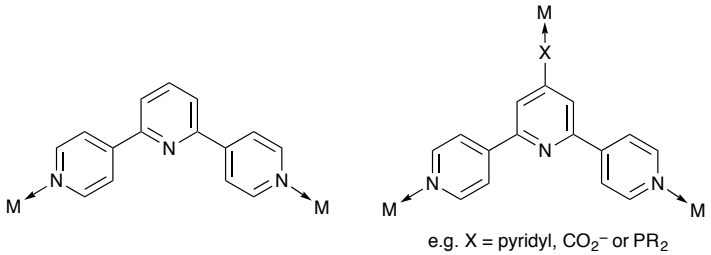

Scheme 1. Divergent coordination modes of 4,2':6',4"-tpy ligands without (left) and with (right) coordinatively non-innocent 4'-substituents.

We recently reported the synthesis of the ditopic ligand 1,4-bis(*n*-octoxy)-2,5-bis(4,2':6',4"-terpyridin-4'-yl)benzene (**1**, Scheme 2) and its reaction with $ZnCl_2$ to produce $[\{Zn_2Cl_4(\mathbf{1})\}\cdot 4H_2O]_n$ comprising 2D→2D parallel interpenetrated (4,4)-

sheets [33]. The long alkyl chains were originally introduced to aid ligand solubility since simple arene spacers between the 4,2':6',4''-tpy domains gave poorly soluble compounds. However, the location of the octoxy chains in extended conformations within the heart of the interpenetrated (4,4)-sheets in $[\{Zn_2Cl_4(\mathbf{1})\}\cdot 4H_2O]_n$ suggested that they may play a significant role in controlling the assembly. Indeed, a systematic study of reactions of $Zn(OAc)_2$ with 4'-(4-ROC_6H_4)-4,2':6',4''-tpy ligands demonstrates that increasing the length of the alkoxy chains switches the assembly from 1D-coordination polymers to discrete molecular complexes [19]. We now report an investigation of the reactions of **1** and its methoxy analogue **2** (Scheme 2) with zinc(II) halides.

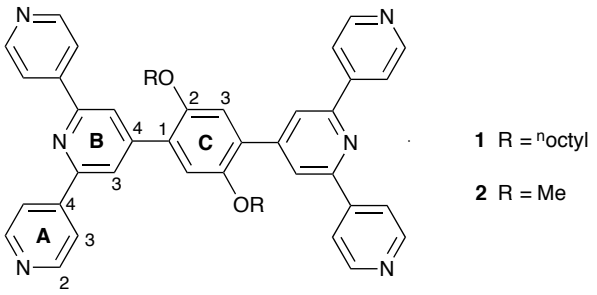

Scheme 2. Structures of **1** and **2** with numbering for NMR assignments.

2 Experimental

2.1 General

^1H and ^{13}C NMR spectra were recorded using a Bruker Avance III-500 NMR spectrometer at 295 K, and chemical shifts are referenced to residual solvent peaks with respect to δ(TMS) = 0 ppm. Electrospray (ESI) and high resolution ESI mass spectra were measured on Bruker Esquire 3000plus and Bruker maXis 4G instruments, respectively. Absorption and IR spectra were recorded on a Varian

Carry 5000 spectrometer and a Shimadzu FTIR-8400S spectrophotometer, respectively.

2,5-Bis(methoxy)benzene-1,4-dicarbaldehyde was bought from Sigma-Aldrich. Compound **1** was prepared as previously reported [33].

*2.2 1,4-Bis(methoxy)-2,5-bis(4,2':6',4''-terpyridin-4'-yl)benzene (**2**)*

4-Acetylpyridine (2.04 g, 16.8 mmol) was added to a solution of 2,5-bis(methoxy)benzene-1,4-dicarbaldehyde (0.80 g, 4.12 mmol) in EtOH (250 mL). KOH pellets (0.93 g, 16.6 mmol) were added in one portion, followed by aqueous NH_3 (25%, 15 mL). The reaction mixture was stirred at room temperature for 20 h. The precipitate that formed was collected by filtration, washed with H_2O and EtOH, and dried in vacuo over P_2O_5. Compound **2** was recrystallized from EtOH/$CHCl_3$ and was isolated as a pale yellow solid (0.81 g, 1.35 mmol, 32.8%). Decomp > 320 ^oC. ^1H NMR (500 MHz, $CDCl_3$) δ / ppm 8.81 (m, 8H, H^{A2}), 8.09 (m, 8H, H^{A3}), 8.07 (s, 4H, H^{B3}), 7.15 (m, 2H, H^{C3}), 3.92 (s, 6H, H^{OMe}). ^{13}C NMR (126 MHz, $CDCl_3$) ∂ / ppm 154.8 (C^{B2}), 150.6 (C^{A2}), 148.1 (C^{C2}), 146.1 (C^{B4}), 129.0 (C^{C1}), 121.3 (C^{B3}), 121.2 (C^{A3}), 114.1 (C^{C3}), 56.6 (C^{OMe}). IR (solid, ν, cm^{-1}) 3079 (w), 3024 (w), 2831 (w), 1696 (w), 1591 (s), 1558 (w), 1541 (w), 1508 (w), 1496 (w), 1397 (w), 1388 (m), 1208 (w), 1181 (w), 1029 (m), 994 (w), 858 (w), 819 (s), 742 (w), 734 (w), 673 (w), 652 (s), 629 (s), 598 (w). ESI-MS *m/z* 601.6 $[M + H]^+$ (base peak, calc. 601.2). HR ESI-MS *m/z* 601.2350 $[M + H]^+$ (base peak, calc. 601.2347). UV-Vis λ / nm (ε / $dm^3\ mol^{-1}\ cm^{-1}$) (CH_2Cl_2, 2.5×10^{-5} mol dm^{-3}) 257 (34300), 316 sh (14550), 340 sh (11200). Satisfactory elemental analysis could not be obtained.

*2.3 [{Zn_2Br_4(**1**)}]*

A solution of **1** (19.9 mg, 0.025 mmol) in $CHCl_3$ (6.0 mL) was prepared in a test tube, and MeOH (3.0 mL) was layered on top, followed by a solution of $ZnBr_2$ (11.3 mg, 0.05 mmol) in MeOH (5.0 mL). The tube was sealed with parafilm and after a month at room temperature, pale yellow crystals had formed. Found C 50.35, H 4.83, N 6.87; $C_{52}H_{56}Br_4N_6O_2Zn_2$ requires C 50.07, H 4.53, N 6.74%.

*2.4 [{Zn_2Br_4(**2**)}·2$C_6H_4Cl_2$]$_n$*

A solution of **2** (15 mg, 0.025 mmol) in $C_6H_4Cl_2$/MeOH (6.0/2.0 mL) was placed in a test tube, and a mixture of $C_6H_4Cl_2$ (1.5 mL) and MeOH (1.5 mL) was layered on top, followed by a solution of $ZnBr_2$ (11.3 mg, 0.05 mmol) in MeOH (5.0 mL). The tube was sealed with parafilm and after a month at room temperature, pale yellow crystals had formed. Found C 44.17, H 3.05, N 8.40; $C_{38}H_{28}Br_4N_6O_2Zn_2$ requires C 43.42, H 2.69, N 8.00%.

*2.5 [{Zn_2I_4(**2**)}·2.3$C_6H_4Cl_2$]$_n$*

A solution of **2** (15 mg, 0.025 mmol) in $C_6H_4Cl_2$/MeOH (6.0/2.0 mL) was prepared in a test tube, and a mixture of $C_6H_4Cl_2$ (1.5 mL) and MeOH (1.5 mL) was layered on top, followed by a solution of ZnI_2 (16.3 mg, 0.05 mmol) in MeOH (5.0 mL). The tube was sealed with parafilm and after a month at room temperature, yellow crystals had formed. Found C 37.69, H 2.51, N 6.71; $C_{38}H_{28}I_4N_6O_2Zn_2$·$C_6H_4Cl_2$ requires C 38.13, H 2.33, N 6.06%.

2.6 Crystallography

Data were collected on a Bruker-Nonius Kappa APEX diffractometer; data reduction, solution and refinement used APEX2 [34] and CRYSTALS [35]. Structural diagrams and structural analysis were carried out using Mercury v. 3.3 [36,37] and TOPOS [38]. SQUEEZE [39] procedure had to be used to treat the solvent region in $[Zn_2Br_4(\mathbf{1})]_n$ and part of the solvent region in $[\{Zn_2Br_4(\mathbf{2})\}\cdot 2C_6H_4Cl_2]_n$ and $[\{Zn_2I_4(\mathbf{2})\}\cdot 2.3C_6H_4Cl_2]_n$.

*2.7 [{Zn$_2$Br$_4$(**1**)}]*

After SQUEEZE: $C_{52}H_{56}Br_4N_6O_2Zn_2$, M = 1247.43, colourless block, monoclinic, space group $C2/c$, a = 20.6639(16), b = 11.9145(10), c = 23.6388(17) Å, β = 92.289(5)°, U = 5815.2(8) Å^3, Z = 4, D_c = 1.425 Mg m^{-3}, μ(Cu-Kα) = 4.549 mm^{-1}, T = 123 K. Total 19113 reflections, 5293 unique, R_{int} = 0.044. Refinement of 3765 reflections (198 parameters) with $I > 2\sigma(I)$ converged at final $R1$ = 0.0607 ($R1$ all data = 0.0808), $wR2$ = 0.0646 ($wR2$ all data = 0.0845), gof = 0.9359.

*2.8 [{Zn$_2$Br$_4$(**2**)}·2C$_6$H$_4$Cl$_2$]$_n$*

After SQUEEZE: $C_{50}H_{36}Br_4Cl_4N_6O_2Zn_2$, M = 1492.06, colourless block, monoclinic, space group $P2_1/n$, a = 12.0911(16), b = 18.972(3), c = 13.5812(18) Å, β = 111.805(5)°, U = 2892.5(4) Å^3, Z = 2, D_c = 1.71 Mg m^{-3}, μ(Cu-Kα) = 7.186 mm^{-1}, T = 123 K. Total 21568 reflections, 5069 unique, R_{int} = 0.030. Refinement of 4994 reflections (307 parameters) with $I > 2\sigma(I)$ converged at final $R1$ = 0.0530 ($R1$ all data = 0.0560), $wR2$ = 0.1358 ($wR2$ all data = 0.1390), gof = 0.9466.

*2.9 [{Zn_2I_4(**2**)}·2.3$C_6H_4Cl_2$]$_n$*

After SQUEEZE: $C_{52}H_{37.50}Cl_{4.50}I_4N_6O_2Zn_2$, M = 1576.32, yellow block, monoclinic, space group $P2_1/n$, a = 11.997(2), b = 19.440(3), c = 13.828(2) Å, β = 112.664(7)°, U = 2976.0(5) Å^3, Z = 2, D_c = 1.76 Mg m^{-3}, μ(Cu-Kα) = 19.476 mm^{-1}, T = 123 K. Total 20800 reflections, 5181 unique, R_{int} = 0.045. Refinement of 5173 reflections (267 parameters) with $I > 2\sigma(I)$ converged at final $R1$ = 0.0683 ($R1$ all data = 0.0733), $wR2$ = 0.1811 ($wR2$ all data = 0.1843), gof = 0.9589.

3 Results and discussion

3.1 Ligand synthesis and characterization

Compound **2** was prepared by the one-pot [21] reaction of four equivalents of 4-acetylpyridine with 2,5-bis(methoxy)benzene-1,4-dicarbaldehyde in EtOH in the presence of NH_3. In the electrospray mass spectrum of **2**, the base peak at *m/z* 601.6 corresponded to the $[M + H]^+$ ion; the high resolution ESI mass spectrum confirmed the formulation with the base peak at *m/z* 601.2350 for $[M + H]^+$ (calculated *m/z* 601.2347). Solution ^{1}H and ^{13}C NMR spectra of **2** were assigned by 2D methods and the ^{1}H NMR spectrum is shown in Figure 1. The aromatic region of the spectrum is little altered on going from **1** (∂ 8.81 (H^{A2}), 8.11 (H^{B3}), 8.09 (H^{A3}) and 7.16 pm (H^{C3})) to **2** (∂ 8.81 (H^{A2}), 8.09 (H^{A3}), 8.07 (H^{B3}) and 7.15 ppm (H^{C3})) and is consistent with the C_2-symmetric structure shown in Scheme 2. The absorption spectrum of **2** is dominated by a broad absorption arising from $\pi^* \leftarrow \pi$ and $\pi^* \leftarrow n$ transitions (λ_{max} = 257 nm) which tails out to ≈440 nm.

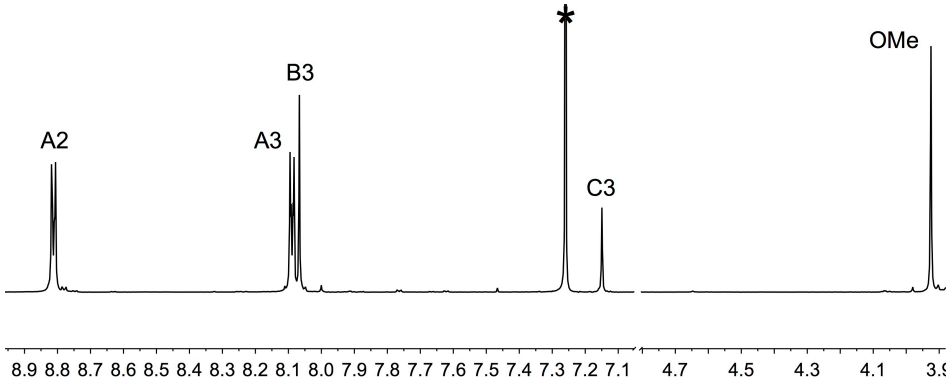

Figure 1. 500 MHz ^{1}H NMR spectrum of **2** ($CDCl_3$); see Scheme 2 for atom labelling. * = residual $CHCl_3$. Chemical shifts in ∂ / ppm.

3.2 Crystal growth

The general approach to crystal growth was by layering a MeOH solution of a zinc(II) halide over either a $CHCl_3$ solution of **1** or a $C_6H_4Cl_2$/MeOH solution of **2**. An intermediate layer of solvent was used to slow down solvent diffusion. Crystallization experiments with a $CHCl_3$ solution of **2** led only to poor quality crystals which readily lost solvent (see later). Crystallization tubes were left standing at room temperature for around a month.

Single crystal diffraction analysis of crystals confirmed a general formula of $[\{Zn_2X_4(L)\}]_n$ for all products. Before submitting for elemental analysis, the crystals were dried under high vacuum. For $[\{Zn_2Br_4(\mathbf{1})\}]_n$, volatile solvents were removed from the lattice, and the bulk material gave satisfactory analysis for $[\{Zn_2Br_4(\mathbf{1})\}]_n$. For the compounds containing **2**, elemental analysis was consistent with $[\{Zn_2Br_4(\mathbf{2})\}]_n$ and $[\{Zn_2Br_4(\mathbf{2})\}]_n{\cdot}C_6H_4Cl_2$, respectively.

*3.3 [{Zn_2Br_4(**1**)}]$_n$*

The coordination polymer [{Zn_2Br_4(**1**)}]$_n$ crystallizes in the monoclinic space group *C*2/*c* with unit cell parameters that are close to those observed for [{Zn_2Cl_4(**1**)}·$4H_2O$]$_n$ [33] (Table 1). The asymmetric unit contains half a molecule of **1** and one $ZnBr_2$ unit, and the repeat unit (with symmetry generated Zn, Br and N atoms) is shown in Figure 2. The alkyl chain is in an extended conformation, but is disordered and has been modelled over two positions of fractional occupancies 0.49 and 0.51. Ligand **1** binds only through the outer pyridine rings, as is typical of 4,2':6',4"-tpys [1] and atom Zn1 is tetrahedrally coordinated; pertinent bond parameters are given in the caption to Figure 2.

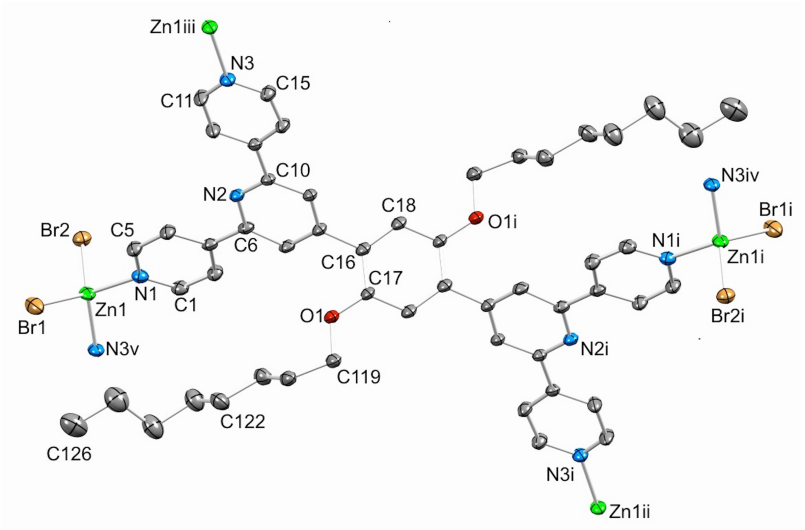

Figure 2. The repeat unit (with symmetry generated connected atoms) in [{Zn_2Br_4(**1**)}]$_n$ (H atoms omitted; ellipsoids plotted at 30% probability level; for the disordered alkyl chain, only one site is shown). Symmetry codes: i = 1–*x*, 2–*y*, 1–*z*; ii = 1–*x*, 1+*y*, $^1/_2$–*z*; iii = *x*, 1–*y*, $^1/_2$+*z*; iv = 1–*x*, 1+*y*, $^3/_2$–*z*; v = *x*, 1–*y*, –$^1/_2$+*z*. Selected bond parameters: Zn1–N1 = 2.044(5), Zn1–$N3^v$ = 2.040(4), Zn1–Br1 = 2.3538(10), Zn1–Br2 = 2.3686(10) Å; $N3^v$–Zn1–Br1 = 107.18(13), $N3^v$–Zn1–Br2 = 106.69(14), Br1–Zn1–Br2 = 123.24(4), $N3^v$–Zn1–N1 = 112.57(18), Br1–Zn1–N1 = 103.51(13), Br2–Zn1–N1 = 103.68(13)°.

Table 1. Comparison of unit cell parameters for crystals of coordination polymers isolated from different crystallization experiments.

Ligand	Solvent for ligand	ZnX_2	Space group	*a* / Å	*b* / Å	*c* / Å	β / °
1	$CHCl_3$	$ZnCl_2$	*C*2/*c*[a]	20.6102(6)	11.5999(6)	23.8198(12)	90.978(3)
1	$CHCl_3$	$ZnBr_2$	*C*2/*c*	20.6639(16)	11.9145(10)	23.6388(17)	92.289(5)
2	$CHCl_3$	$ZnCl_2$	$P2_1/c$[b]	12.862(5)	20.409(7)	12.847(4)	114.01(3)
2	MeOH/$C_6H_4Cl_2$	$ZnBr_2$	$P2_1/n$	12.0911(16)	18.972(3)	13.5812(18)	111.805(5)
2	MeOH/$C_6H_4Cl_2$	ZnI_2	$P2_1/n$	11.997(2)	19.440(3)	13.828(2)	112.664(7)

[a]Reference [33]. [b]Preliminary data; see text.

Propagation of the coordination polymer in $[\{Zn_2Br_4(\mathbf{1})\}]_n$ generates (4,4) nets containing metallomacrocycles constructed from four zinc(II) centres, two 4,2':6',4"-tpy domains from two different ligands **1** (coloured purple in Figure 3) and two half-ligands **1** (dark green in Figure 3). This mimics the assembly in $[\{Zn_2Cl_4(\mathbf{1})\}\cdot 4H_2O]_n$ that we have already discussed in detail [33]. Each ditopic ligand **1** acts as a 4-connecting node, the node coinciding with the centroid of the arene spacer (ring C in Scheme 2). Since the second half of each ligand **2** is generated by inversion, the 4-connecting node is necessarily planar. Each sheet has a corrugated topology (Figure 4a) and the octoxy chains are accommodated along the middle of the sheet (Figure 4).

The corrugated sheets are relatively open, and this allows them to interpenetrate [40] in a 2D→2D parallel fashion [41,42]. Figure 5 shows a TOPOS [38] representation of the structure, showing the 2D→2D parallel interpenetration and the nesting of adjacent sheets with the $ZnBr_2$ units accommodated in the V-shaped cavities in the next layer. Each net is conveniently considered as a 2-nodal net (i.e. 4-connecting ligand **1**, and 2-connecting Zn atom). However, it may be simplified to a (4,4)-descriptor because the 4-connecting nodes can either be

connected through a loop (i.e. Zn atom) or a straight line. Topologically, the nets are identical. However, since the interpenetration occurs through the loops, it is useful to retain the Zn atoms as nodes [43].

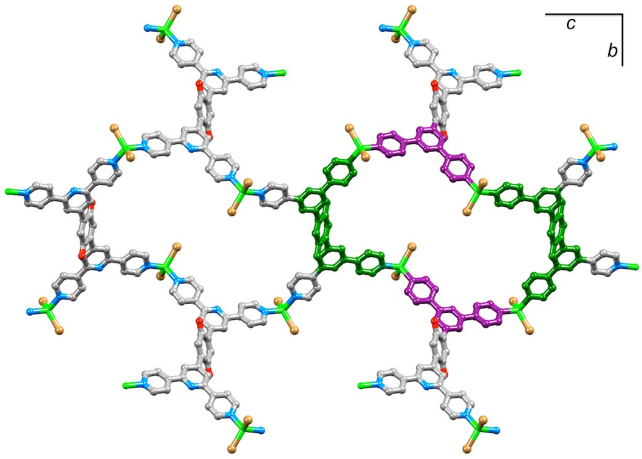

Figure 3. Formation of metallomacrocyclic units in each (4,4) net in $[\{Zn_2Br_4(\mathbf{1})\}]_n$. Octyl chains and H atoms are omitted for clarity.

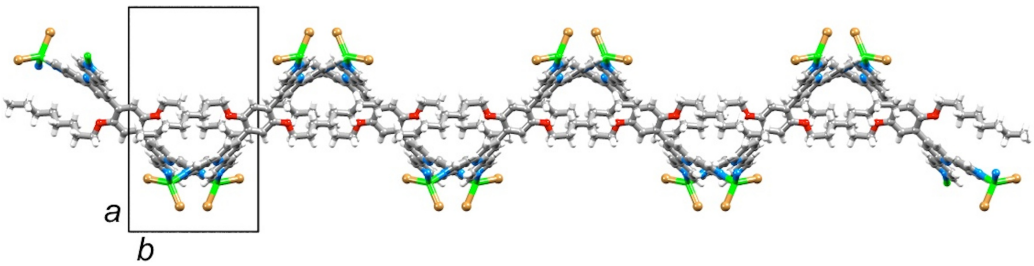

(a)

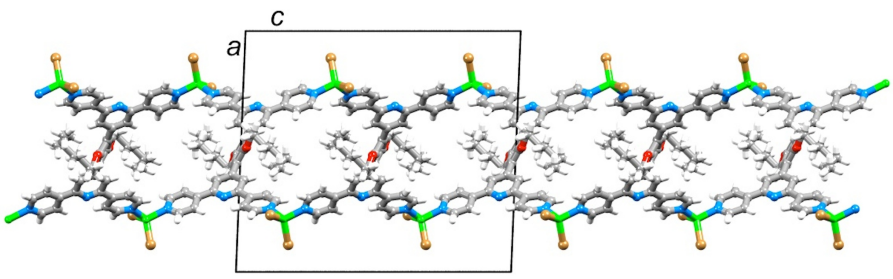

(b)

Figure 4. Part of one (4,4) sheet in $[\{Zn_2Br_4(\mathbf{1})\}]_n$ viewed down the (a) *c*-axis, and (b) *b*-axis showing alignment of the octoxy chains within the sheet.

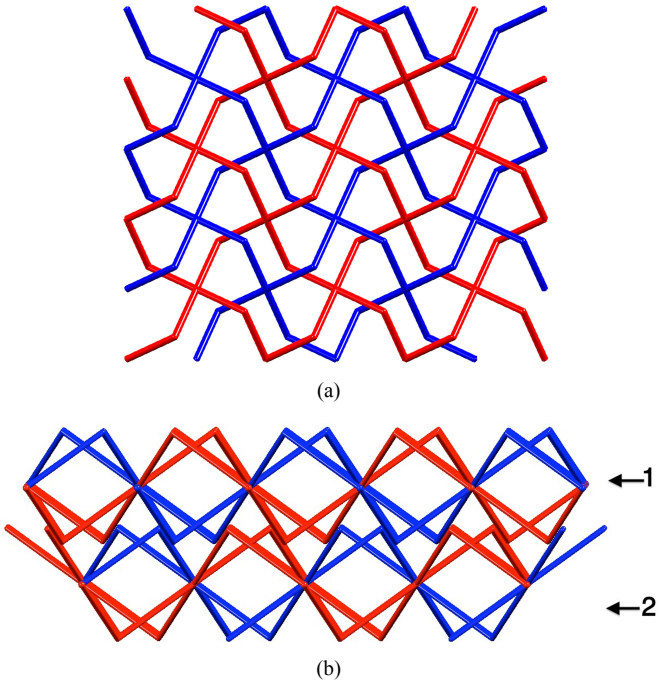

Figure 5. TOPOS representations of (a) 2D→2D parallel interpenetrating sheets, and (b) nesting of two adjacent layers (labelled 1 and 2 for clarity) in $[\{Zn_2Br_4(\mathbf{1})\}]_n$.

3.4 $[\{Zn_2Br_4(\mathbf{2})\}\cdot 2C_6H_4Cl_2]_n$ and $[\{Zn_2I_4(\mathbf{2})\}\cdot 2.3C_6H_4Cl_2]_n$

In both $[\{Zn_2Cl_4(\mathbf{1})\}\cdot 4H_2O]_n$ [33] and $[\{Zn_2Br_4(\mathbf{1})\}]_n$, the octoxy chains are threaded through the 2D→2D parallel interpenetrating sheets and appear to play a role in stabilizing the interpenetrated structural motifs. We therefore decided to investigate the effects of removing the chains. For solubility reasons, we replaced the octoxy groups by methoxy substituents, rather than using a simple phenylene spacer between the 4,2':6',4"-tpy domains. Initially, single crystals were grown from layering a $CHCl_3$ solution of **2** over a MeOH solution of $ZnCl_2$. However, crystal quality was poor and rapid solvent loss made handling the crystals difficult. Preliminary data (Table 1) suggested that the product crystallized in the monoclinic space group $P2_1/c$ and that ligand **2** behaves as a 4-connecting node generating a repeat unit similar to that present in $[\{Zn_2Br_4(\mathbf{1})\}]_n$ (Figure 2).

A change of solvent for the ligand in the crystallization experiments from $CHCl_3$ to a 1 : 1 mixture of MeOH and $C_6H_4Cl_2$ (see Experimental section) resulted in the growth of X-ray quality crystals of $[\{Zn_2Br_4(\mathbf{2})\}\cdot 2C_6H_4Cl_2]_n$ and $[\{Zn_2I_4(\mathbf{2})\}\cdot 2.3C_6H_4Cl_2]_n$. Problems with solvent disorder necessitated the use of SQUEEZE [39] to treat part of the solvent region in both structure determinations. In the discussion below, only the resolved solvent molecules are considered. Both $[\{Zn_2Br_4(\mathbf{2})\}\cdot 2C_6H_4Cl_2]_n$ and $[\{Zn_2I_4(\mathbf{2})\}\cdot 2.3C_6H_4Cl_2]_n$ crystallize on the monoclinic space group $P2_1/n$ and cell parameters for the two coordination polymers are comparable (Table 1). They are also similar to the cell parameters for the preliminary structure of the product of **2** with $ZnCl_2$ (Table 1).

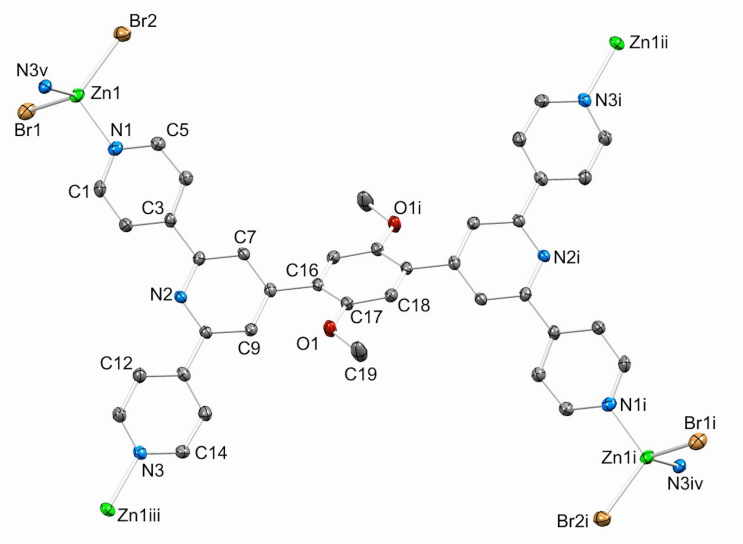

Fig. 6. The repeat unit (with symmetry generated connected atoms) in $[\{Zn_2Br_4(\mathbf{2})\}\cdot 2C_6H_4Cl_2]_n$ (H atoms omitted; ellipsoids plotted at 40% probability level). Symmetry codes: i = $-1-x$, $1-y$, $-z$; ii = $-{}^3/_2+x$, ${}^3/_2-y$, $-{}^1/_2+z$; iii = ${}^1/_2-x$, $-{}^1/_2+y$, ${}^1/_2-z$; iv = $-{}^3/_2+x$, ${}^1/_2-y$, $-{}^1/_2+z$; v = ${}^1/_2-x$, ${}^1/_2+y$, ${}^1/_2-z$. Selected bond lengths and angles: Zn1–N^v = 2.050(4), Zn1–Br1 = 2.3503(8), Zn1–Br2 = 2.3665(8), Zn1–N1= 2.046(4) Å; $N3^v$–Zn1–Br1 = 109.00(11), $N3^v$–Zn1–Br2 = 103.86(10), Br1–Zn1–Br2 = 120.66(3), $N3^v$–Zn1–N1 = 105.18(14), Br1–Zn1–N1 = 108.78(11), Br2–Zn1–N1 = 108.27(11)°.

Figure 6 shows the repeat unit within the coordination network of $[\{Zn_2Br_4(\mathbf{2})\}\cdot 2C_6H_4Cl_2]_n$. The asymmetric unit contains half a molecule of **2** and one $ZnBr_2$ unit, and the second half of ligand **2** is generated by inversion. Bond parameters for the tetrahedrally coordinated atom Zn1 are given in the caption to Figure 6. Ligand **2** acts as a planar 4-connecting node and propagation into a single sheet follows the same connectivity pattern as described above for $[\{Zn_2Br_4(\mathbf{1})\}]_n$. Figure 7a illustrates the metallomacrocycles in the 2D-sheet, and a comparison with Figure 3 demonstrates that the assemblies are analogous in terms of connectivities. However, comparing Figure 7b with Figure 4a reveals that the profiles of the corrugated sheets in the two 2D-coordination polymers are different. Firstly, the methoxy substituents point towards the top and bottom of the 2D-sheet, compared to the orientations of the octoxy chains along the sheet. Secondly, whereas 4-connecting nodes along each row in a sheet are coplanar in $[\{Zn_2Br_4(\mathbf{2})\}\cdot 2C_6H_4Cl_2]_n$, they are tilted in $[\{Zn_2Br_4(\mathbf{1})\}]_n$ giving rise to the two profiles shown in Figures 8a and 8b, respectively. Figure 7 shows a TOPOS [38] representation of part of one sheet in $[\{Zn_2Br_4(\mathbf{2})\}\cdot 2C_6H_4Cl_2]_n$, for comparison with Figure 5a. The coordination network in $[\{Zn_2I_4(\mathbf{2})\}\cdot 2.3C_6H_4Cl_2]_n$ is essentially isostructural with that in $[\{Zn_2Br_4(\mathbf{2})\}\cdot 2C_6H_4Cl_2]_n$. Within the tetrahedral zinc(II) coordination sphere, Zn–I bond distances are 2.445(6) and 2.5488(12) Å, and Zn–N bond lengths are 2.065(5) and 2.063(5) Å; the N–Zn–N3 and I–Zn–I bond angles are 105.9(2) and 108.63(13)^o, and N–Zn–I bond angles lie in the range 108.6(2) to 115.0(2)^o.

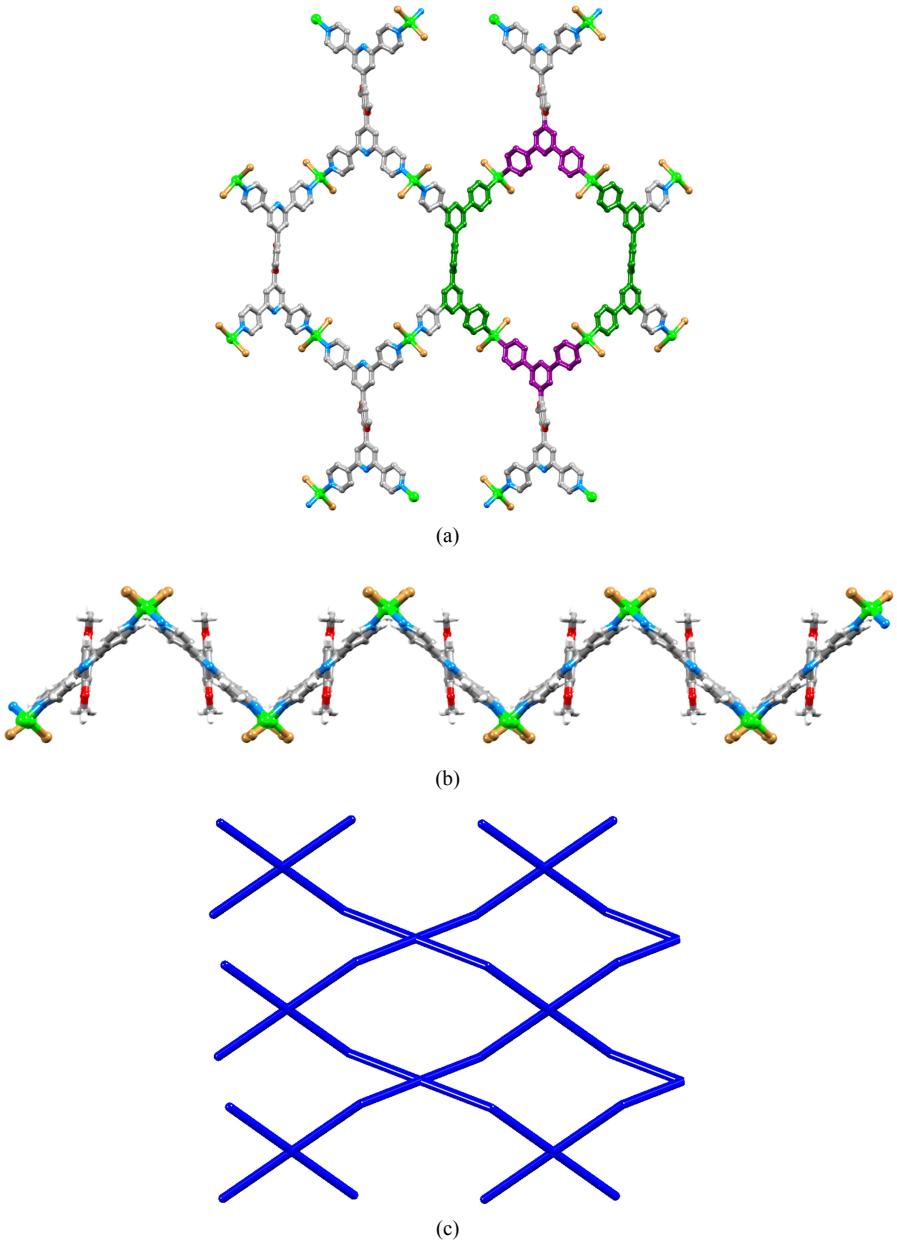

Fig. 7. (a) Formation of metallomacrocyclic units in each (4,4) net in $[\{Zn_2Br_4(\mathbf{2})\}\cdot 2C_6H_4Cl_2]_n$; the colour coding is the same as in Fig. 3. (b) Part of one corrugated (4,4) sheet in $[\{Zn_2Br_4(\mathbf{2})\}\cdot 2C_6H_4Cl_2]_n$ (compare with Fig. 4a). (c) TOPOS representation of part of one sheet in $[\{Zn_2Br_4(\mathbf{2})\}\cdot 2C_6H_4Cl_2]_n$.

In contrast to the nesting of sheets in $[\{Zn_2Br_4(\mathbf{1})\}]_n$ (Figure 5b), the corrugated sheets in $[\{Zn_2Br_4(\mathbf{2})\}\cdot 2C_6H_4Cl_2]_n$ and $[\{Zn_2I_4(\mathbf{2})\}\cdot 2.3C_6H_4Cl_2]_n$ associate closely through face-to-face π-interactions of 4,2':6',4"-tpy domains. This is shown for

$[\{Zn_2Br_4(\mathbf{2})\}\cdot 2C_6H_4Cl_2]_n$ in Figure 9; analogous interactions occur in the iodido derivative. In $[\{Zn_2Br_4(\mathbf{2})\}\cdot 2C_6H_4Cl_2]_n$, the angles between the least squares planes of pairs of bonded pyridine rings are 6.2 and 17.3°, compared to 4.7 and 19.4° in $[\{Zn_2I_4(\mathbf{2})\}\cdot 2.3C_6H_4Cl_2]_n$. π-Stacking occurs between the least twisted bipyridine-domains of adjacent ligands. For the π-stacking interactions shown in Figure 9, the interplane (least squares planes through the bpy units) separation is 3.38 Å in $[\{Zn_2Br_4(\mathbf{2})\}\cdot 2C_6H_4Cl_2]_n$ and 3.48 Å in $[\{Zn_2I_4(\mathbf{2})\}\cdot 2.3C_6H_4Cl_2]_n$; the corresponding inter-centroid separation are 3.59 and 3.68 Å. The dichlorobenzene molecules fit neatly into the remaining cavities (Figure 10), with aromatic face-to-face and edge-to-face interactions playing a principal role. The inclusion of arene solvent molecules appears to be an important factor during crystallization; crystals with apparently analogous lattices to $[\{Zn_2Br_4(\mathbf{2})\}]_n$ and $[\{Zn_2I_4(\mathbf{2})\}]$ but grown from $CHCl_3$/MeOH and using **2** with $ZnCl_2$ were very sensitive to solvent loss (see above).

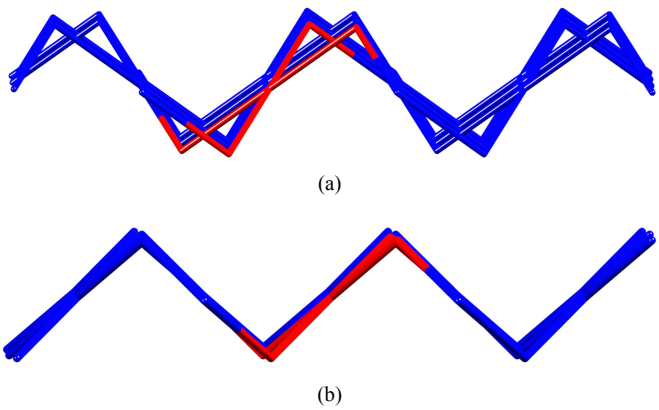

Figure 8 Comparison of part of one (4,4)-net in (a) $[\{Zn_2Br_4(\mathbf{2})\}\cdot 2C_6H_4Cl_2]_n$ and (b) $[\{Zn_2Br_4(\mathbf{1})\}]_n$ with one 4-connecting node shown in red.

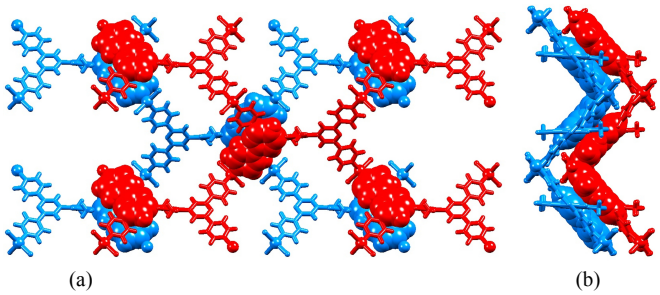

Figure 9. Inter-sheet face-to-face π-interactions in $[\{Zn_2Br_4(\mathbf{2})\}\cdot 2C_6H_4Cl_2]_n$.

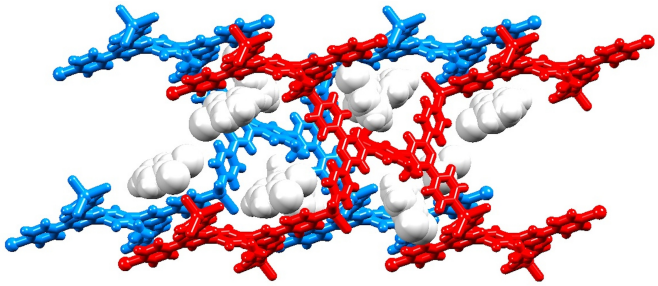

Figure 10. Accommodation of $C_6H_4Cl_2$ molecules in cavities in the lattice of $[\{Zn_2Br_4(\mathbf{2})\}\cdot 2C_6H_4Cl_2]_n$.

4. Conclusions

The effects of reducing the length of the alkoxy substituents in the ditopic ligands **1** (octoxy) to **2** (methoxy) on reactions with zinc(II) halides has been investigated. Crystallization by layering using a MeOH solution of $ZnBr_2$ and $CHCl_3$ solution of **1** leads to $[\{Zn_2Br_4(\mathbf{1})\}]_n$; ligand **1** acts as a planar 4-connecting node which consists of (4,4)-nets each with a corrugated topology. The open nature of the net results in 2D→2D parallel interpenetration, with extended octoxy chains running through the middle of the sheets. Layering of 1,2-$C_6H_4Cl_2$ solutions of **2** with $ZnBr_2$ or ZnI_2 resulted in the formation of $[\{Zn_2Br_4(\mathbf{2})\}\cdot 2C_6H_4Cl_2]_n$ and $[\{Zn_2I_4(\mathbf{2})\}\cdot 2.3C_6H_4Cl_2]_n$ which contain 2-dimensional (4,4)-nets. These coordination polymers are essentially isostructural and the (4,4)-nets possess a

corrugated topology. However, structural features of the sheets are different from those in $[\{Zn_2Br_4(\mathbf{1})\}]_n$. The methoxy substituents in $[\{Zn_2Br_4(\mathbf{2})\}\cdot 2C_6H_4Cl_2]_n$ and $[\{Zn_2I_4(\mathbf{2})\}\cdot 2.3C_6H_4Cl_2]_n$ point above and below the sheet, and adjacent sheets engage in face-to-face π-interactions. In contrast to the 2D→2D parallel interpenetration in $[\{Zn_2Cl_4(\mathbf{1})\}\cdot 4H_2O]_n$ [33] and $[\{Zn_2Br_4(\mathbf{1})\}]_n$, $[\{Zn_2Br_4(\mathbf{2})\}\cdot 2C_6H_4Cl_2]_n$ and $[\{Zn_2I_4(\mathbf{2})\}\cdot 2.3C_6H_4Cl_2]_n$ consist of single sheets. In the latter, the inclusion of arene solvent molecules is an important stabilizing influence.

Appendix 1 Supplementary data

Crystallographic data have been deposited with the CCDC (Cambridge Crystallographic Data Centre, 12 Union Road, Cambridge CB2 1EZ, UK; fax +44 1223 336 033; e-mail: deposit@ccdc.cam.ac.uk or www: http://www.ccdc.cam.ac.uk) and may be obtained free of charge on quoting the deposition numbers CCDC 1038251, 1038252 and 1038253.

Acknowledgements

We thank the Swiss National Science Foundation (grant 200020_149067), the European Research Council (Advanced Grant 267816 LiLo) and the University of Basel for financial support. Maximilian Klein is gratefully acknowledged for his work with the program TOPOS to generate Figures 5, 7c and 8.

References

[1] C. E. Housecroft, Dalton Trans. 43 (2014) 6594.

[2] M.-Y. Wu, K. Zhou, J. Pan, M.-C. Hong, Dalton Trans. 42 (2013) 9954.

[3] E. C. Constable, C. E. Housecroft, M. Neuburger, S. Vujovic, J. A. Zampese, Polyhedron 60 (2013) 120.

[4] Y.-Q. Chen, G.-R. Li, Z. Chang, Y.-K. Qu, Y.-H. Zhang, X.-H. Bu, Chem. Sci. 4 (2013) 3678.

[5] F. Yuan, J. Xie, H.-M. Hu, C.-M. Yuan, B. Xu, M.-L. Yang, F.-X. Dong and G.-L. Xue, CrystEngComm, 2013, 15, 1460.

[6] Y.-Q. Chen, G.-R. Li, Y.-K. Qu, Y.-H. Zhang, K.-H. He, Q. Gao, X.-H. Bu, Cryst. Growth Des. 13 (2013) 901.

[7] E. C. Constable, C. E. Housecroft, J. Schönle, S. Vujovic, J. A. Zampese, Polyhedron 62 (2013) 260.

[8] F. Yuan, Q.-E. Zhu, H.-M. Hu, J. Xie, B. Xu, C.-M. Yuan, M.-L. Yang, F.-X. Dong,G.-L. Xue, Inorg. Chim. Acta 397 (2013) 117.

[9] H.-N. Zhang, F. Yuan, H.-M. Hu, S.-S. Shen, G.-L. Xue, Inorg. Chem. Comm. 34 (2013) 51.

[10] E. C. Constable, C.E. Housecroft, S. Vujovic, J. A. Zampese, A. Crochet, S. R. Batten, CrystEngComm 15 (2013) 10068.

[11] J. Granifo, R. Gavino, E. Freire, R. Baggio, J. Mol. Struct. 1063 (2014) 102.

[12] J. Yang, S.-W. Yan, X. Wang, D.-R. Xiao, H.-Y. Zhang, X.-L. Chi, J.-L. Zhang, E.-B. Wang, Inorg. Chem. Comm. 38 (2013) 100.

[13] Y. Li, Z. Ju, B. Wu, D. Yuan, Cryst. Growth Des. 13 (2013) 4125.

[14] M.-S. Wang, M.-X. Li, X. He, M. Shao, Z.-X. Wang, Inorg. Chem. Comm. 42 (2014) 38.

[15] E. C. Constable, C. E. Housecroft, S. Vujovic, J. A. Zampese, CrystEngComm 16 (2014) 328.

[16] E. C. Constable, C. E. Housecroft, A. Prescimone, S. Vujovic, J. A. Zampese, CrystEngComm 16 (2014) 8691.

[17] Y. M. Klein, E. C. Constable, C. E. Housecroft, J. A. Zampese, Polyhedron 81 (2014) 98.

[18] Y. M. Klein, E. C. Constable, C. E. Housecroft, A. Prescimone, Inorg. Chem. Comm. 49 (2014) 41.

[19] Y. M. Klein, E. C. Constable, C. E. Housecroft, J. A. Zampese, A. Crochet, CrystEngComm 16 (2014) 9915.

[20] F. Kröhnke, Synthesis (1976) 1.

[21] J. Wang, G. S. Hanan, Synlett (2005) 1251.

[22] E. C. Constable, A. M. W. Cargill Thompson, P. Harveson, L. Macko, M. Zehnder, Chem. Eur. J. 1 (1995) 360.

[23] Y. Yan, J. Huang, Coord. Chem. Rev. 254 (2010) 1072.

[24] M. Wang, C. Wang, X.-Q. Hao, J. Liu, X. Li, C. Xu, A. Lopez, L. Sun, M.-P. Song, H.-B. Yang, X. Li, J. Am. Chem. Soc. 136 (2014) 6664.

[25] T.-Z. Xie, K. Guo, M. Huang, X. Lu, S.-Y. Liao, R. Sarkar, C. N. Moorefield, S. Z. D. Cheng, C. Wesdemiotis, G. R. Newkome, Chem. Eur. J. 20 (2014) 11291.

[26] A. Schultz, X. Li, C. E. McCusker, C. N. Moorefield, F. N. Castellano, C. Wesdemiotis, G. R. Newkome, Chem. Eur. J. 18 (2012) 11569.

[27] X. Lu, X. Li, Y. Cao, A. Schultz, J.-L. Wang, C. N. Moorefield, C. Wesdemiotis, S. Z. D. Cheng, G. R. Newkome, Angew. Chem. Int. Ed. 52 (2013) 7728.

[28] O. Johansson, L. Eriksson, R. Lomoth, Dalton Trans. (2008) 3649.

[29] A. Harriman, A. Mayeux, A. De Nicola, R. Ziessel, Phys. Chem. Chem. Phys. 4 (2002) 2229.

[30] G. W. V. Cave, C. L. Raston, J. Chem. Soc., Perkin Trans. 1 (2001) 3258.

[31] J. Yoshida, S.-I. Nishikiori, H. Yuge, J. Coord. Chem., 2013, 66, 2191.

[32] S. A. S. Ghozlan and A. Z. A. Hassanien, Tetrahedron, 2002, 58, 9423.

[33] E. C. Constable, C. E. Housecroft, S. Vujovic and J. A. Zampese, CrystEngComm, 2014, 16, 3494.

[34] Bruker Analytical X-ray Systems, Inc., 2006, APEX2, version 2 User Manual, M86-E01078, Madison, WI.

[35] P. W. Betteridge, J. R. Carruthers, R. I. Cooper, K. Prout, D. J. Watkin, J. Appl. Cryst. 36 (2003) 1487.

[36] I. J. Bruno, J. C. Cole, P. R. Edgington, M. K. Kessler, C. F. Macrae, P. McCabe, J. Pearson, R. Taylor, Acta Crystallogr. 58B (2002) 389.

[37] C. F. Macrae, I. J. Bruno, J. A. Chisholm, P. R. Edgington, P. McCabe, E. Pidcock, L. Rodriguez-Monge, R. Taylor, J. van de Streek, P. A. Wood, J. Appl. Cryst. 41 (2008) 466.

[38] V. A. Blatov, A. P. Shevchenko, TOPOS Professional v. 4.0, Samara State University, Russia.

[39] A. L. Spek, Acta Crystallogr. 65 D (2009) 148.

[40] H. Guo, D. Qiu, X. Guo, S. R. Batten, H. Zhang, CrystEngComm 11 (2009) 2611.

[41] S. R. Batten in Supramolecular Chemistry: From Molecules to Nanomaterials, eds. P. A. Gale, J. W. Steed, Wiley, Chichester, 2012, vol. 6, p. 3107.

[42] S. R. Batten, CrystEngComm 18 (2001) 1.

[43] S. R Batten, S. M. Neville, D. R. Turner, Coordination Polymers: Design, Analysis and Applications, RSC Publishing, 2008, Chapter 2.